Progress In Electromagnetics Research, PIER 91, 243–258, 2009

STUDY ON THE DEMODULATION STRUCTURE OF READER RECEIVER IN A PASSIVE RFID ENVIRONMENT

J.-H. Bae, W. Choi, J. Kim, G.-Y. Choi, and J.-S. Chae

RFID/USN Research Department
Electronics and Telecommunications Research Institute (ETRI)
138 Gajeongno, Yuseong-gu, Daejeon 305–700, Korea

Abstract—In this paper, we present a demodulation structure suitable for a reader receiver in a passive Radio Frequency IDentification (RFID) environment. In a passive RFID configuration, undesirable DC-offset phenomenon may appear in the baseband of the reader receiver. As a result, this DC-offset phenomenon can severely degrade the performance of the extraction of valid information from a received signal in the reader receiver. To mitigate the DC-offset phenomenon, we propose a demodulation structure to reconstruct a corrupted signal with the DC-offset phenomenon, by extracting useful transition information from the corrupted signal. It is shown that the proposed method can successfully detect valid data from a received signal, even when the received baseband signal is distorted with the DC-offset phenomenon.

1. INTRODUCTION

A passive Radio Frequency IDentification (RFID) refers to a technology which uses radio communications to contactlessly identify a tagged physical object [1, 2]. Essentially, a passive RFID system consists of a reader and a passive tag without a battery. The International standard, ISO 18000-6C defines the communication protocol and Ultra High Frequency (UHF) band between the reader and the passive tag [3, 4]. Many researches related to the UHF RFID field have been conducted, as described in [5–8]. In case of the passive RFID technology, a reader must provide continuous radio power to a tag while the tag sends its information to the reader. This

Corresponding author: J.-H. Bae (baejh@etri.re.kr).

is done so the tag can use an Amplitude-Shift-Keying (ASK) or a Phase-Shift-Keying (PSK) modulation of the reflected power, namely backscatter modulation, from the tag antenna instead of actively using a radio transmitter [2–4]. However, if sufficient isolation between a transmitter and a receiver is not guaranteed and a perfect matching is not accomplished between an antenna and a RF-front end in the reader side, the transmission power (Tx power) created by the reader transmitter may leak to the receiver (Fig. 1(a)) [2]. Because of this unwanted leakage in a reader receiver, DC-offset phenomenon can be observed in a baseband of the reader receiver. As a result, the received baseband signal can be corrupted by the DC-offset phenomenon (Fig. 1(b)). Case 1 and Case 2 of Fig. 1(b) are measured baseband signals in our reader receiver using the Agilent Logic Analyzer.

In order to detect valid information from the corrupted signal, we propose a demodulation structure composed of an edge signal generator and an edge detector to successfully decode the received signal distorted by the DC-offset phenomenon. This paper is organized as follows. In Section 2, we formulate the problem of interest for a passive RFID environment. In Section 3, we describe the demodulation structure and the method to extract meaningful information from the distorted signal with DC-offset phenomenon in detail. In Section 4, we show the simulation examples. Finally, we draw our conclusions in Section 5.

2. PROBLEM FORMULATION

In this section, we introduce a general DC-offset noise model to mathematically express the DC-offset phenomenon in a passive RFID environment. A modulated signal from a tag may be distorted by the DC-offset phenomenon caused by the leakage components in a reader receiver (Fig. 1). Considering this phenomenon, DC-offset noise can be expressed as follows:

$$n_{dc}(t) = A_{dc} \cdot e^{-B \cdot t} e^{j(w_d \cdot t + \psi)} \tag{1}$$

where A_{dc} is an initial DC-offset value, $e^{-B \cdot t}$ and $e^{jw_d \cdot t}$ represent a damping term and an oscillation term of the DC-offset noise, and $e^{j\psi}$ is the initial phase of the DC-offset noise. Increasing the constant B in the damping term leads to a rapid reduction of the DC-offset noise, whereas decreasing the constant B leads to a slow decrease of the DC-offset noise, as t increases. Meanwhile, increasing w_d in the oscillation term means that the DC-offset noise fluctuates with a high frequency. On the other hand, decreasing w_d means that the DC-offset noise fluctuates with a low frequency. By adjusting the parameters A_{dc},

B, and w_d related to the DC-offset noise to proper values, any kind of DC-offset phenomenon in the field of passive RFID can be established. Therefore, if we define a transmitted signal waveform, DC-offset noise, and a received signal as $s(t)$, n_{dc}, and $r(t)$, then the input signal in the reader receiver can be written as follows:

$$\begin{aligned} r(t) &= s(t) \cdot e^{-j\left(\frac{2\pi \cdot f_c}{c} \cdot r_k + \theta_0\right)} + n_{dc}(t) + n(t) \\ &= s(t) \cdot e^{j\theta} + n_{dc}(t) + n(t) \\ &= \underbrace{\mathrm{Re}\{r(t)\}}_{In\text{-}phase} + j \cdot \underbrace{\mathrm{Im}\{r(t)\}}_{Quadrature\text{-}phase} = r_I(t) + j \cdot r_Q(t) \end{aligned} \tag{2}$$

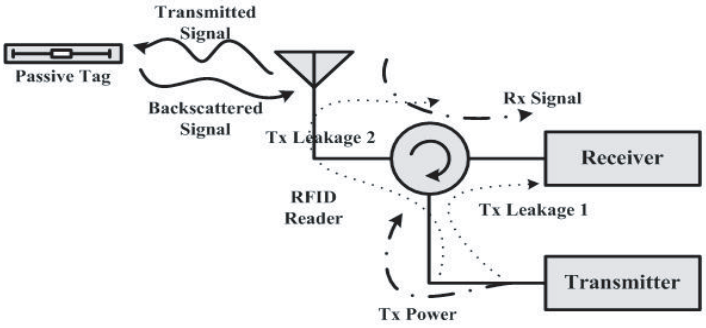

(a)

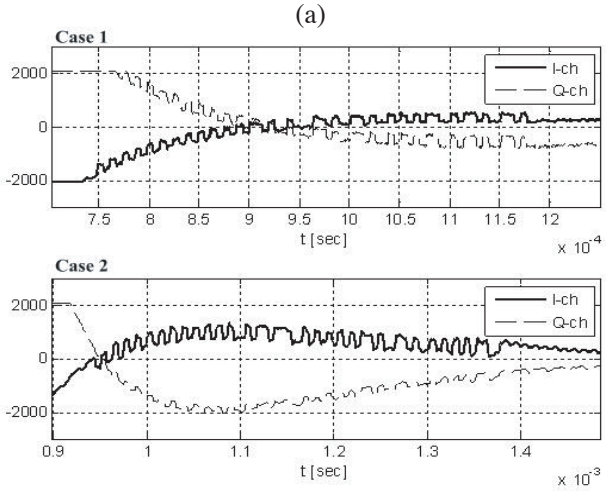

(b)

Figure 1. Description of leakage components and the corresponding DC-offset phenomenon in a passive RFID configuration.

where, f_c is a carrier frequency, r_k is a reading distance between a reader and a tag, c is the propagation velocity, θ_0 is an initial phase of the transmitted tag signal, and $n(t)$ is the complex additive noise, which is a sample function of a white Gaussian process with power spectrum $N_0/2$ watts/hertz. As described in Eq. (2), the received signal, $r(t)$ has a complex signal form, which is composed of an in-phase channel (I-channel) signal, $r_I(t)$ and a quadrature-phase channel (Q-channel) signal, $r_Q(t)$. The reason is that the phase θ of a backscattering signal from a tag to a reader is periodically varied according to the reading distance, r_k in UHF passive RFID communication. Fig. 2 shows the I-channel and the Q-channel received signals with DC-offset noise using Eq. (1) and Eq. (2).

FM0 (bi-phase space)-encoded signal with the symbol duration of $T_b = 12.5\,\mu$sec is considered for this example. A data-0 and a data-1 of the FM0 signaling are expressed in [3, 4]. For the DC-offset noise, we set the initial DC-offset A_{dc} to 5, the constant of damping term B

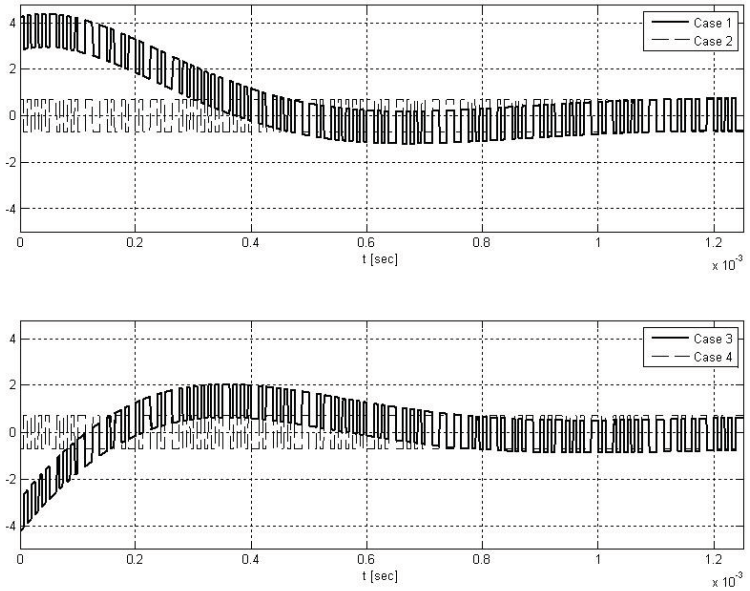

Figure 2. I-channel and Q-channel FM0 received signals distorted by DC-offset noise when the number of FM0 symbols is 100. Case 1 and Case 3 represent the I-channel and the Q-channel received signals with DC-offset noise. Case2 and Case 4 represent the I-channel and the Q-channel received signals without DC-offset noise.

to $T_s/T_b \cdot 100$, and the constant of oscillation term w_d to $1/(T_b \cdot 100)$.

When the corrupted signal of Fig. 2 is received in a traditional reader receiver, the performance of the reader receiver can be dramatically degraded (Fig. 3). Fig. 3(a) shows the well-known receiver structure with signal correlators and an optimal detector [9, 10]. Fig. 3(b) represents the error rate performance of the FM0 encoded signal (p_e) at several values of Signal-to-Noise Ratio (SNR), where the SNR is defined as the ratio E/N_0. In the following section, we describe a demodulation structure and the method to mitigate the DC-offset noise which can occur in passive RFID configuration.

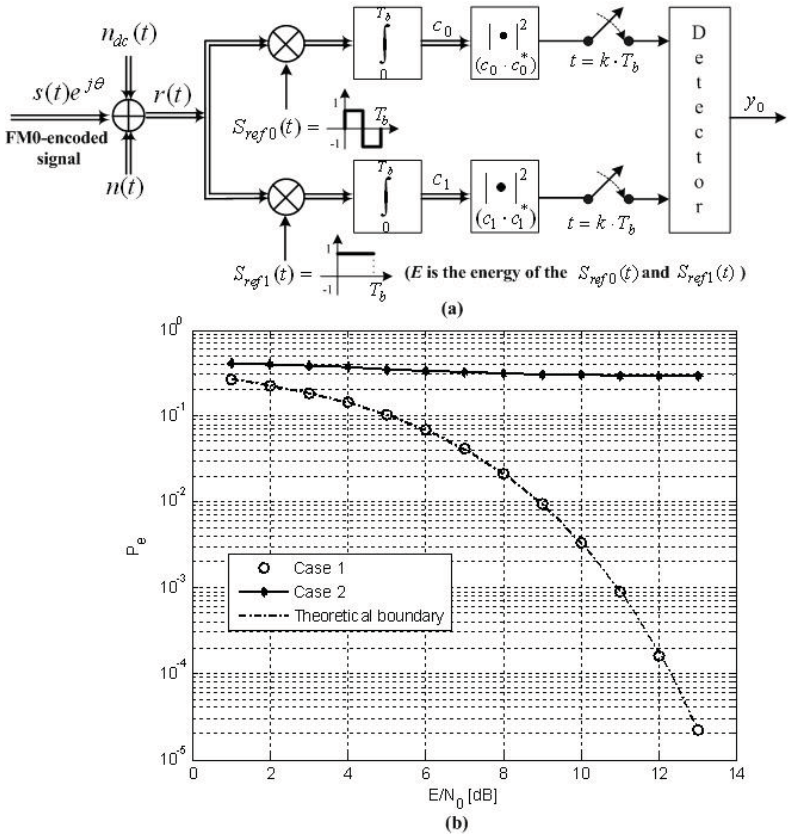

Figure 3. The error rate performance as to DC-offset noise for a traditional receiver with optimal detector. Case 1 denotes the p_e without DC-offset noise. Case 2 denotes the p_e with DC-offset noise.

3. DEMODULATION ALGORITHM

In this section, we introduce a demodulation structure and the algorithm to be suitable for the reconstruction of a distorted signal with DC-offset noise. In our method, we make use of the signal transitions from a received signal to reduce DC-offset noise and to enhance a valid factor of the signal at the same time. Fig. 4 shows the proposed demodulation architecture, which primarily includes an edge signal generator, an edge extractor, and a signal reconstruction block.

In order to generate an edge signal with respect to the received signal $r(t)$, an initial edge signal is designed using a predefined $g_m(t)$ as follows:

$$y_{e1}(t) = \underbrace{\left| r_I(t) \otimes g_m(t) \right|}_{I\text{-}channel} + \underbrace{\left| r_Q(t) \otimes g_m(t) \right|}_{Q\text{-}channel} \tag{3}$$

where, $g_m(t)$ has the shape similar to the data-0 of FM0 signal and is defined as follows:

$$g_m(t) = \left[\frac{4}{\pi} \sum_{n=1}^{N_m} \frac{\sin(2\pi \cdot (2n-1) \cdot t/T_b)}{(2n-1)} \right]_{, t=\left(k \cdot \frac{T_b}{n_s}\right),\ k=0,1,2,\ldots,n_s-1} \tag{4}$$

where the received signal is sampled at a sampling rate of $n_s/T_b = 1/T_s$ (n_s is an integer). The reason for selecting this type of $g_m(t)$ is that the $g_m(t)$ has no DC component in the frequency domain and the $g_m(t)$ can be also used to generate a desired edge signal at every transition in a received signal through Eq. (3). In the case of the design of the $g_m(t)$, N_m determines the shape of $g_m(t)$. If the value of N_m is decreased, the shape of the $g_m(t)$ is similar to that of a sine waveform. In contrast, the form of the $g_m(t)$ becomes to that of a rectangular pulse by increasing the value of N_m. Of course, a certain differentiator can be also applied to extract transition information from the received signal [11]. However, the performance of the differentiator may be easily degraded when noise is present. Namely, the differentiator may need to have a high *SNR* to achieve good performance. Therefore, it is preferable for us to adopt the concept of integration rather than that of differentiation for the design of the edge signal in the demodulation structure.

In the second step, the generated initial edge signal $y_{e1}(t)$ is reconstructed by removing the low level noise included in a specific level of the initial edge signal. This operation is implemented in the level decision block by using a reference level (Fig. 4). The reference level is generated in the adaptive level generator (Fig. 4). In this case,

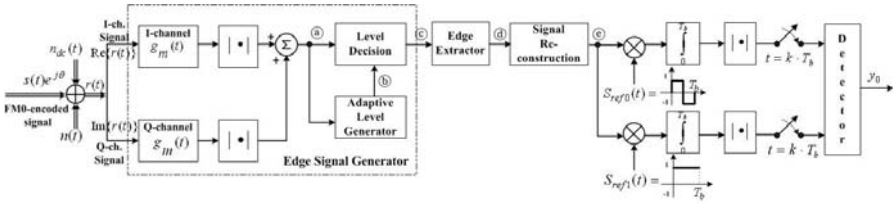

Figure 4. Proposed demodulation structure for the purpose of the reconstruction of a distorted signal with DC-offset noise.

a moving average (MA) model is applied to build the reference level, which can be adaptively changed according to amplitude variations of the initial edge signal. Therefore, the adaptive reference level can be calculated as follows:

$$y_{ref}(t) = \frac{1}{A_m}\sum_{k=1}^{N_w}[y_{e1}(t) + y_{e1}(t - T_s) + y_{e1}(t - 2 \cdot T_s) + \ldots + y_{e1}(t - k \cdot T_s)] \tag{5}$$

where, A_m denotes a gain of the MA and directly determines the specific level of the y_{ref}. N_w is the order of the MA and determines a window size, $W_m = N_w \cdot T_s$, for averaging incoming data. Then, the final edge signal can be obtained after the level decision by using the calculated adaptive reference level and the initial edge signal as follows:

$$y_{e2}(t) = \begin{cases} y_{e1}(t), & y_{e1} \geq y_{ref} \\ 0, & y_{e1} < y_{ref} \end{cases} \tag{6}$$

In the next step, the following edge detection algorithm is used to extract peak positions from the edge signal $y_{e2}(t)$ (Fig. 5), and the operation of the algorithm is carried out in the edge extractor (Fig. 4). According to the algorithm, the positions of the peaks are obtained when a slope of the edge signal is changed from positive to negative using the ∇y_u and ∇y_d.

Finally, according to the following state diagram, a baseband signal without DC-offset noise is regenerated using the extracted edges in the signal reconstruction block.

The procedure for the proposed demodulation method is summarized as follows:

Step 1: The initial edge signal $y_{e1}(t)$ for a corrupted received signal is generated by Eq. (3).

Step 2: To eliminate low level noise contamination in the initial edge signal, the edge signal $y_{e2}(t)$ is regenerated by using both the

initial edge signal and the computed adaptive level as given in Eq. (5) and Eq. (6).

Step 3: The edge information for the edge signal $y_{e2}(t)$ is extracted using the edge detection algorithm (Fig. 5).

Step 4: From the extracted edges, the baseband signal without DC-offset noise is regenerated in the signal reconstruction block (Fig. 4).

Step 5: Finally, the detector decides bit data from the reconstructed signal of Step 4 (Fig. 4).

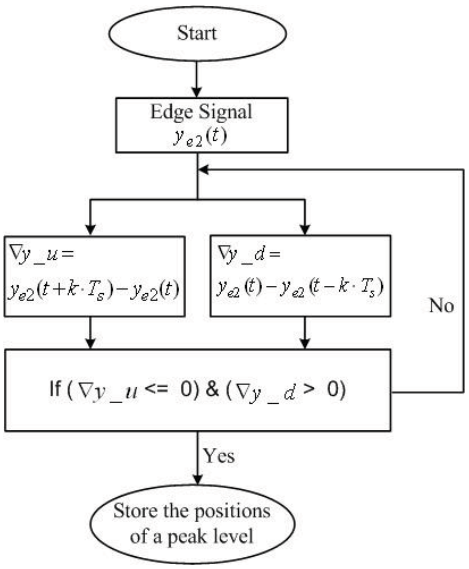

Figure 5. Edge detection algorithm to extract edge information from the created edge signal.

4. SIMULATION RESULTS

In this section, we will show a few examples to demonstrate the performance of the demodulation structure in Section 3. To generate the edge signal with respect to a received signal, it is necessary to determine in advance the design parameters, N_m, A_m, and N_w as defined in Eq. (4) and Eq. (5). The $g_m(t)$ in Eq. (4) has a form of the Fourier series expansion for the data-0 of FM0 and has the fundamental frequency $1/T_b$. As N_m decreases, the $g_m(t)$ is similar to the shape of a sine waveform, resulting in a filtering effect. Due to noise $n(t)$, local peaks can be observed in the edge signal and these local peaks can

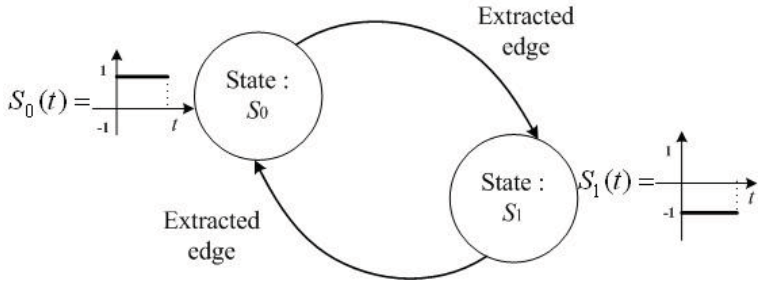

Figure 6. State diagram for generating a signal without DC-offset noise.

degrade the performance of the edge extractor. Therefore, decreasing the value of N_m may cause the local peaks included in the edge signal to be reduced. Fig. 7 shows the error rate p_e for the variation of N_m. In this example, DC-offset noise was not considered and the reference level was fixed to a pre-defined appropriate value instead of using the adaptive reference level. As shown in Fig. 7, we observe that the error rate performance can be improved as the value of N_m is decreased. Next, Fig. 8 shows the error rate p_e for several G_m parameters, when the window size W_m is varied over several values. In this example, N_m is set to a value of 1. G_m is defined as follows: $G_m = N_w/A_m$. From

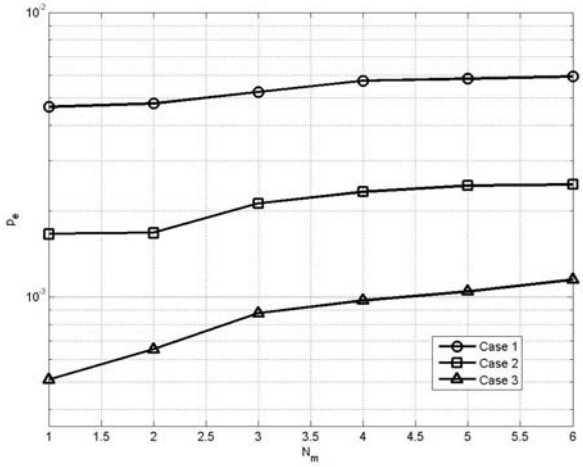

Figure 7. error rate performance as to several values of N_m parameter. Case 1: p_e vs. N_m (SNR =13dB). Case 2: p_e vs. N_m (SNR =14 dB). Case 3: p_e vs. N_m (SNR =15 dB).

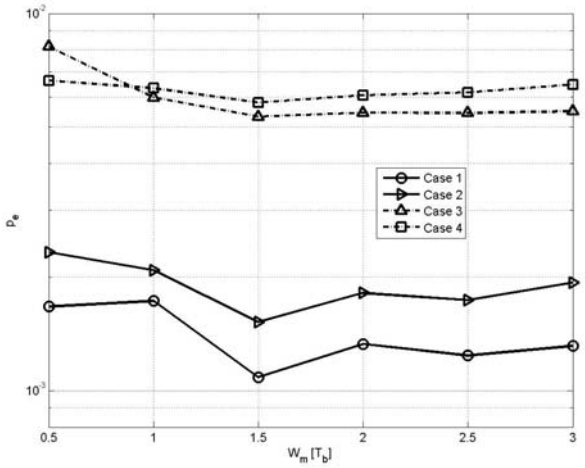

Figure 8. The error rate performance as to several values of W_m parameter. Case 1: p_e vs. W_m with $G_m = 0.88$ ($SNR = 16\,\mathrm{dB}$). Case 2: p_e vs. W_m with $G_m = 0.92$ ($SNR = 16\,\mathrm{dB}$). Case 3: p_e vs. W_m with $G_m = 0.88$ ($SNR = 14\,\mathrm{dB}$). Case 4: p_e vs. W_m with $G_m = 0.92$ (SNR =14 dB).

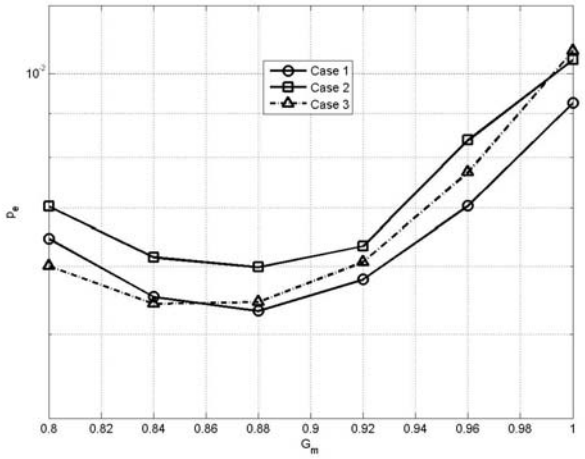

Figure 9. The error rate performance as to several values of G_m parameter. Case 1: p_e vs. G_m with $W_m = 1.0[T_b]$ ($SNR = 14\,\mathrm{dB}$). Case 2: p_e vs. G_m with $W_m = 1.5[T_b]$ ($SNR = 14\,\mathrm{dB}$). Case 3: p_e vs. G_m with $W_m = 2.0[T_b]$ ($SNR = 14\,\mathrm{dB}$).

this definition, $G_m = 1$ means a normalized gain of the reference level. The p_e for all G_m parameters decrease respectively as the W_m increases (Fig. 8). However, there is no noticeable decrease of p_e, although the W_m increases to a value larger than $1.5T_b$. In other words, for W_m values larger than about $1.5T_b$, there is no further reduction of the p_e, although the computational complexity can be increased. In contrast, Fig. 9 shows the p_e for several W_m parameters when the G_m is varied over several values. In this example, N_m is also set to a value of 1. From the result of Fig. 9, the value of $G_m \approx 0.88$, slightly smaller than the normalized value of 1, is appropriate for the optimal value. Using the above results, in order to design the edge signal in the proposed method, it is reasonable to choose W_m as 1.5 times the one symbol duration of the FM0, G_m as 0.88, and N_m as 1, in the context of the error rate performance and the computational complexity.

For the first example, we consider the operation of the proposed demodulation structure when a received signal is the distorted FM0-encoded signal with DC-offset noise in Fig. 2. For this example, the same results of $N_m = 1$, $W_m \approx 1.5T_b$, and $G_m \approx 0.88$ obtained in the above paragraph are applied to construct the edge signal $y_{e2}(t)$. The

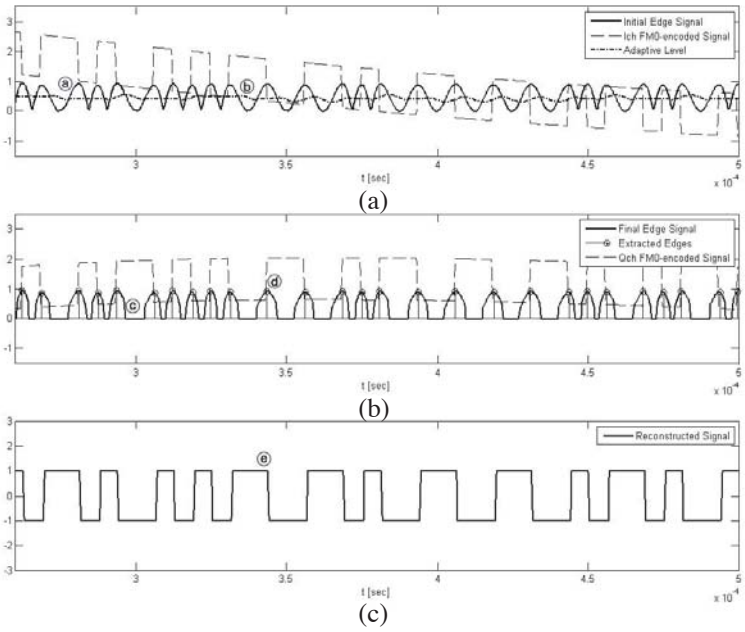

Figure 10. Operation results of the proposed demodulation structure in Fig. 4.

simulation results of the first example are shown in Fig. 10. Fig. 10(a) represents the generated initial edge signal $y_{e1}(t)$ and the corresponding reference level. From Fig. 10(a), the variation of the peak levels of the initial edge signal is very small, while the I-channel received signal is severely fluctuated by DC-offset noise. Fig. 10(b) represents the final edge signal $y_{e2}(t)$ and the extracted edges. We observe that the edge signal $y_{e2}(t)$ is generated at every transition for the received signal. Finally, Fig. 10(c) denotes the regenerated FM0 signal without DC-offset noise.

We also implemented the proposed structure using the VHDL (VHSIC Hardware Description Language) and simulated the operation of the structure using a commercial design software tool (ModelSim SE 6.0), as shown in Fig. 11. Measured FM0 signals (Fig. 1(b) Case 1) are considered for this example. As shown in Fig. 10 and Fig. 11, we observe that the proposed method can successfully reconstruct a corrupted signal, even though the received signal is distorted by DC-offset phenomenon.

For the second example, we compare the performance of the proposed method with that of the traditional method in terms of the error rate p_e. The Monte-Carlo simulation is implemented to estimate the error rate performance. Fig. 12 shows the error rate performances for several SNRs, when only the initial DC-offset value

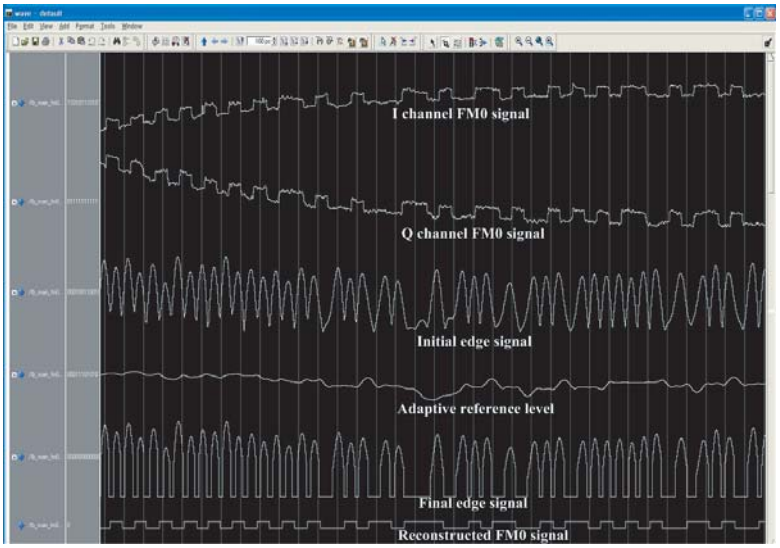

Figure 11. Timing simulation of the proposed demodulation structure.

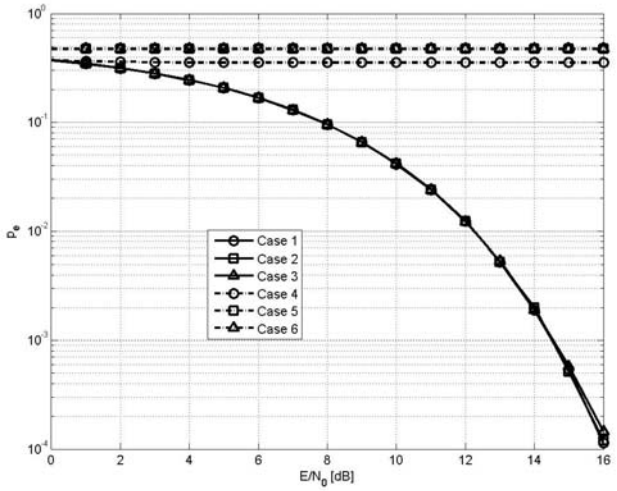

Figure 12. Comparison of the error rate performances between the traditional method and the proposed method when only the initial DC-offset value is considered for the FM0 signal with 100 symbols. Case 1: p_e vs. SNR when $A_{dc} = 1.5,\ B = 0$, and $w_d = 0$, respectively (proposed structure). Case 2: p_e vs. SNR when $A_{dc} = 5,\ B = 0$, and $w_d = 0$, respectively (proposed structure). Case 3: p_e vs. SNR when $A_{dc} = 15,\ B = 0$, and $w_d = 0$, respectively (proposed structure). Case 4: p_e vs. SNR when $A_{dc} = 1.5,\ B = 0$, and $w_d = 0$, respectively (traditional structure). Case 5: p_e vs. SNR when $A_{dc} = 5,\ B = 0$, and $w_d = 0$, respectively (traditional structure). Case 6: p_e vs. SNR when $A_{dc} = 15,\ B = 0$, and $w_d = 0$, respectively (traditional structure).

A_{dc} is considered for generating DC-offset noise. As shown in Fig. 12, the error rate performance with the proposed method can be improved as SNR is increased while the performance with the traditional method cannot. In addition, there is no degradation of the performance with the proposed method, even though the variation of the value of A_{dc} is from one and a half times to fifteen times the amplitude of the received signal. Fig. 13 shows the error rate performances for several SNRs when the DC-offset noise is varied according to W_d. For this example, the initial DC-offset value and the damping term of the DC-offset noise are fixed, as described in Fig. 13. Compared to the result in Fig. 12, the performance of the proposed method slightly can be affected adversely when the oscillation frequency of the DC-offset noise is increased. However, the error rate performance with the proposed method can be also improved as SNR is increased. Meanwhile, we observe that the

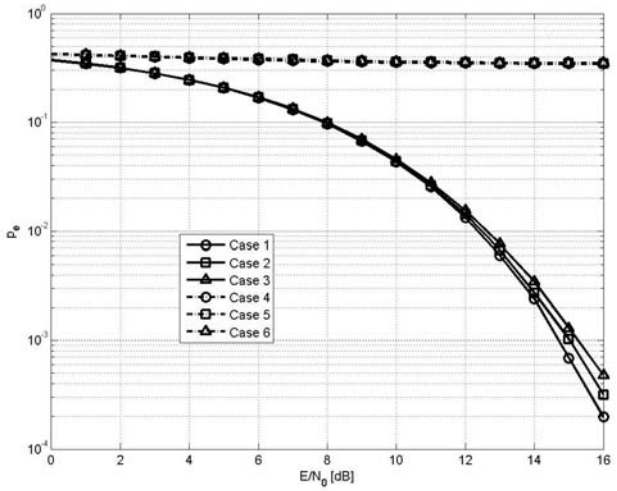

Figure 13. Comparison of the error rate performances between the traditional method and the proposed method when DC-offset noise is considered for the FM0 signal with 100 symbols. Case 1: p_e vs. SNR when $A_{dc} = 10$, $B = T_s/T_b \cdot 80$, and $w_d = 1/(T_b \cdot 100)$, respectively (proposed structure). Case 2: p_e vs. SNR when $A_{dc} = 10$, $B = T_s/T_b \cdot 80$, and $w_d = 1/(T_b \cdot 66.7)$, respectively (proposed structure). Case 3: p_e vs. SNR when $A_{dc} = 10$, $B = T_s/T_b \cdot 80$, and $w_d = 1/(T_b \cdot 50)$, respectively (proposed structure). Case 4: p_e vs. SNR when $A_{dc} = 10$, $B = T_s/T_b \cdot 80$, and $w_d = 1/(T_b \cdot 100)$, respectively (traditional structure). Case 5: p_e vs. SNR when $A_{dc} = 10$, $B = T_s/T_b \cdot 80$, and $w_d = 1/(T_b \cdot 66.7)$, respectively (traditional structure). Case 6: p_e vs. SNR when $A_{dc} = 10$, $B = T_s/T_b \cdot 80$, and $w_d = 1/(T_b \cdot 50)$, respectively (traditional structure). .

traditional method can no longer maintain its performance (Fig. 13). From the results of Fig. 12 and Fig. 13, it can be pointed out that the demodulation structure using the edge signal and the edge extractor can reliably reconstruct a corrupted received signal with DC-offset noise in the passive RFID environment.

5. CONCLUSION

In this study, the DC-offset phenomenon is modeled for a passive RFID environment and is used to evaluate the proposed demodulation method. In order to design the demodulation structure suitable for the passive RFID reader receiver with the DC-offset phenomenon,

transition information using the edge signal and the edge extractor is applied to reconstruct the distorted signal with the DC-offset phenomenon. The Results show that the proposed method can successfully extract valid information from the corrupted signal with DC-offset noise which can occur in passive RFID configuration.

ACKNOWLEDGMENT

This work was supported by the IT R&D program of MKE/IITA [Development of Next Generation RFID Technology for Item Level Applications], Rep. of Korea.

REFERENCES

1. Finkenzeller, K., *RFID Handbook — Fundamentals and Applications in Contactless Smart Cards and Identification*, John Wiley & Sons Ltd, 2003.
2. Dobkin, D. M., *The RF in RFID*, Elsevier Inc., 2008.
3. "EPC radio-frequency identity protocols Class-1 Generation-2 UHF RFID protocol for communications at 860 MHz ∼ 960 MHz version 1.1.0," EPCglobal, 2007.
4. "Radio-frequency identification for item management — Part 6: Parameters for air interface communications at 860 MHz to 960 MHz," ISO/IEC 18000-6C, 2007.
5. Fan, Z. G., S. Qiao, J. T. Huangfu, and L. X. Ran, "Signal descriptions and formulations for long range UHF RFID readers," *Progress In Electromagnetics Research*, PIER 71, 109–127, 2007.
6. Kim, D.-Y., J.-G. Yook, H.-G. Yoon, and B.-J. Jang, "Interference analysis of UHF RFID systems," *Progress In Electromagnetics Research B*, Vol. 4, 115–126, 2008.
7. Shi, X.-L., X.-W. Shi, Q.-L. Huang, and F. Wei, "An enhanced binary anti-collision algorithm of backtracking in RFID system," *Progress In Electromagnetics Research B*, Vol. 4, 263–271, 2008.
8. Loo, C.-H., et al., "Chip impedance matching for UHF RFID tag antenna design," *Progress In Electromagnetics Research*, PIER 81, 359–370, 2008.
9. Proakis, J. G., M. Salehi, and G. Bauch, *Contemporary Communication Systems Using MATALB & Simulink*, 2nd edition, Thomson-Brooks/Cole, 2004.
10. Haykin, S., *Communication Systems*, 4th edition, John Wiley & Sons, Inc., 2001.

11. Tan, A. and C. E. Saavedra, "A binary phase shift keying demodulator using pulse detection," *IEEE International Conference on Electrical and Electronics Engineering*, 2004.